



# Triggering of the Hinlopen/Yermak Megaslide in relation to paleoceanography and climate history of the continental margin north of Spitsbergen

Daniel Winkelmann and Ruediger Stein

*Alfred Wegener Institute for Polar and Marine Research, Columbusstrasse, D-27568 Bremerhaven, Germany  
([dwinkelmann@awi-bremerhaven.de](mailto:dwinkelmann@awi-bremerhaven.de))*

[1] On the basis of the detailed sedimentological record of the key-core PS66/309-1 and a review of open literature, we present an assessment of the paleoenvironmental conditions as well as trigger mechanism of the Hinlopen/Yermak Megaslide north of Spitsbergen. The Svalbard archipelago is characterized by strong inflow of Atlantic water accompanied by rapidly falling sea level, rapidly growing Svalbard-Barents Sea-Ice Sheet, and associated increasing glaciotectonic activity during the time window around 30 calendar kyr B. P. of this catastrophic failure event. Thus the potential trigger mechanisms include sediment buoyancy and excess pore pressure, hydrate stability, and tectonic/glaciotectonic processes. While the common scenarios seem to fail to explain this unique submarine megaslide, we focus on glacial processes and their consequences for the regional tectonic framework. We conclude that the Hinlopen/Yermak Megaslide has been the consequence of the rapid onset of Late Weichselian glaciation resulting in a drastic sea level drop, asymmetrical ice loading, and a forebulge development leading to enhanced tectonic movements along the Hinlopen fault zone. As the final trigger we assume a strong earthquake positioned below or close to the SE Sophia Basin.

**Components:** 8962 words, 7 figures, 1 table.

**Keywords:** slope stability; submarine slides; Svalbard; Arctic Ocean; Sophia Basin; MIS 3.

**Index Terms:** 3070 Marine Geology and Geophysics: Submarine landslides; 0726 Cryosphere: Ice sheets; 1641 Global Change: Sea level change (1222, 1225, 4556); 3002 Marine Geology and Geophysics: Continental shelf and slope processes (4219); 3075 Marine Geology and Geophysics: Submarine tectonics and volcanism.

**Received** 14 September 2006; **Revised** 30 March 2007; **Accepted** 26 April 2007; **Published** 29 June 2007.

Winkelmann, D., and R. Stein (2007), Triggering of the Hinlopen/Yermak Megaslide in relation to paleoceanography and climate history of the continental margin north of Spitsbergen, *Geochem. Geophys. Geosyst.*, 8, Q06018, doi:10.1029/2006GC001485.

## 1. Introduction

[2] Causes of submarine slides and factors that control slide frequencies remain poorly understood despite the fact that submarine slides represent a hazard to seafloor structures and are able to generate tsunamis with far-reaching consequences

[e.g., *Baptista et al.*, 1998; *Bondevik et al.*, 1997, 2005; *Garcia et al.*, 2003]. On the European glacially influenced continental margins, slide frequency has been related to repeated ice sheet advances to the shelf [*Haflidason et al.*, 2005] implying a lithologic and thus climate-dependent control. Theories that tried to associate submarine

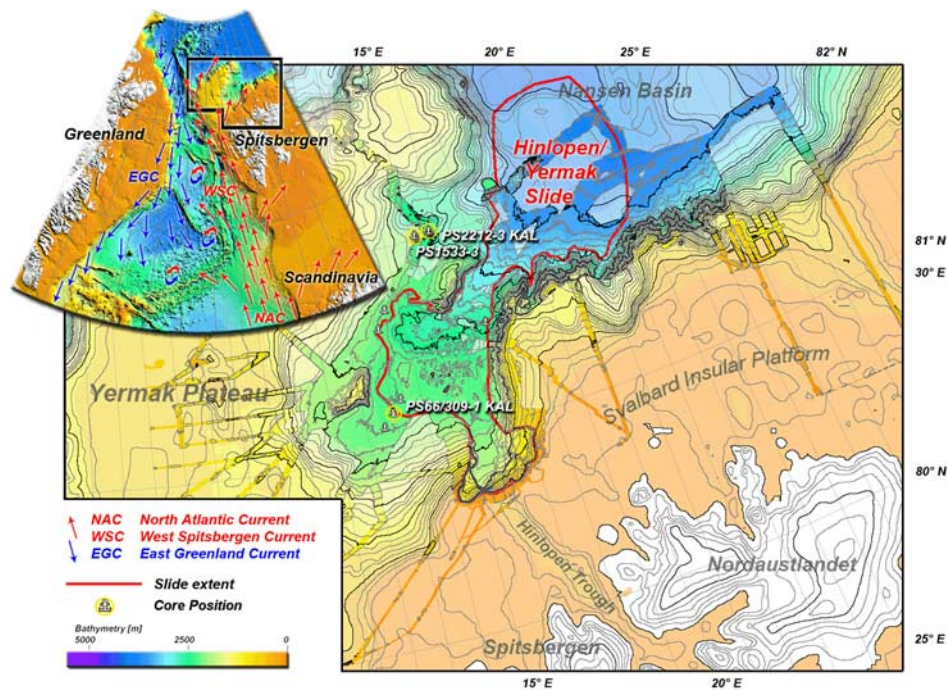


**Figure 1.** Overview map of the Spitsbergen area with (modern) oceanic circulation, ice sheet extent during Saalian and Weichselian Glaciations, LGM (according to *Landvik et al.* [1998] and *Svendsen et al.* [2004]) and ice streams (according to *Ottesen et al.* [2005]), location of cores, and extent of the Hinlopen/Yermak Megaslide (according to *Winkelmann et al.* [2006a, 2006b]). Bathymetry: high-resolution Swath bathymetry [*Winkelmann et al.*, 2006a; *Vanneste et al.*, 2006] on IBCAO [*Jakobsson et al.*, 2001].

slides to sea level changes range from falling to rising sea level scenarios [e.g., *McMurtry et al.*, 2004; *Mienert et al.*, 2005b; *Haflidason et al.*, 2005], from highstand to low stand sea level. This paper deals with a major submarine slide that occurred on the continental slope north of Svalbard first described by *Cherkis et al.* [1999]. To give credit to the source area (Hinlopen Trough and Trough Mouth Fan) and the deposition area of the megaslide (east and southeast of the Yermak Plateau) (see below), we propose to name it “Hinlopen/Yermak Megaslide.” On the basis of the description of *Winkelmann et al.* [2004, 2006a] (Figure 1), this slide can be classified as a megaslide and it represents an end-member concerning geometrical parameters like headwall heights, volume, size and geometry of slid blocks. In this paper we present new constraints on environmental and paleoceanographic conditions of this area with focus on the most likely environmental conditions that favored the triggering of the highly dynamic catastrophic first slide event of the Hinlopen/Yermak Megaslide.

### 1.1. Modern Oceanographic Setting

[3] The modern surface water circulation pattern around Spitsbergen is characterized by the northward flowing West Spitsbergen Current (WSC). It transports warm and saline Atlantic water into the Arctic Ocean via Fram Strait where it branches into the North Svalbard Current (NSC) flushing the shelf of NW and north Spitsbergen, the Yermak Plateau Current (YPC) and the Yermak Slope Current (YSC) that follows the bathymetric contours of the submarine plateau into the Arctic Ocean [*Schlichtholz and Houssais*, 1999a, 1999b; *Schauer et al.*, 2004]. East Greenland Current (EGC), as counterpart to the WSC, transports colder and less saline Arctic water into the Greenland Sea (Figure 1).

### 1.2. Glacial History of the Study Area

[4] The Svalbard archipelago with its main islands Spitsbergen and Nordaustlandet was repeatedly affected by major glaciations during the Weichselian [*Mangerud et al.*, 1998; *Svendsen et al.*, 2004]. Extent and character of these glaciations have been extensively studied and summarized within the

**Table 1.** Dating Results for Core PS66/309-1 KAL<sup>a</sup>

Sample ID	Core Depth, cm	14C-Age B. P.	Corr. 14C-Age B. P.	Calendar Age B. P.	Dated Material
KIA 25699	088–091	15660 ± 70	15240 ± 70	18541 ± 237	<i>N. pachyderma sin.</i>
KIA 29238	142–144	20020 ± 140	19600 ± 140	23379 ± 394	<i>N. pachyderma sin.</i>
KIA 25700	179–182	25390 ± 200	24970 ± 200	29928 ± 310	<i>N. pachyderma sin.</i>
KIA 30396	182–184	25310 ± 210	24890 ± 210	29876 ± 312	<i>N. pachyderma sin.</i>
KIA 27116	299–302	42340 ± 2020	41920 ± 2020	45858 ± 1898	<i>N. pachyderma sin.</i>

<sup>a</sup> Water depth 2270 m; recovery 765 cm. AMS radiocarbon dating was on carbonaceous shells of *Neogloboquadrina pachyderma sinistralis* at the Leibniz-Labor for Radiometric Dating and Isotope Research in Kiel, Germany. Conversion to calendar ages was done using the CalPal online software (<http://www.calpal-online.de>) with the CalPal2005\_SFCP calibration curve. A standard reservoir age of 420 years has been applied for all dates.

QUEEN (Quaternary Environments of the Eurasian North) project [e.g., *Svendsen et al.*, 2004, and references therein]. The Hinlopen/Yermak Megaslide headwall is situated on the continental shelf between Spitsbergen and Nordaustlandet islands which are separated by a deeply routed fault zone along which persistent glacial erosion has formed a cross-shelf trough. This Hinlopen cross shelf trough hosted an ice stream during glacial times, and probably also during the Last Glacial Maximum (LGM) [*Ottesen et al.*, 2005]. In contrast to other cross shelf troughs, the termination of the Hinlopen trough is characterized by a number of submarine slide headwalls that form the Hinlopen/Yermak Megaslide [*Cherkis et al.*, 1999; *Vanneste et al.*, 2004, 2006; *Winkelmann et al.*, 2006a, 2006b] rather than a Trough Mouth Fan (TMF).

## 2. Material and Methods

[5] Detailed bathymetric data and high-resolution ground-penetrating echo sounding data were acquired by the HYDROSWEEP DS2 and the PARASOUND Hydromap Control systems, respectively, aboard R/V *Polarstern* during cruise ARKXX/3 [*Stein*, 2005]. Additional data were collected during cruises ARKXV/2 of R/V *Polarstern* [*Jokat*, 2000] and R/V *Jan Mayen* [*Vanneste et al.*, 2004, 2006]. Preliminary data compilation on the structure of the Hinlopen/Yermak Megaslide were performed by *Winkelmann et al.* [2006a, 2006b]. On the basis of the PARASOUND record, coring sites were selected along a representative key-profile crossing the well developed marginal facies of the mega slide during cruise ARKXX/3 [*Stein*, 2005; *Winkelmann et al.*, 2006a]. Multisensor core logging, core description, x-ray radiography and standard geological sampling were performed aboard R/V *Polarstern* [*Stein*, 2005]. IRD was counted according to *Grobe* [1987]. Core PS66/309-1 KAL was sampled con-

tinuously at 2–3 cm intervals for stable isotope analysis of *N. pachyderma (sin.)* Stable oxygen and carbon isotopes were measured by standard techniques [*Duplessy*, 1978] on the automated Carbo-Kiel device connected to a Finnigan MAT 251 mass spectrometer. The external analytical reproducibility is 0.08‰ and 0.04‰ for  $\delta^{18}\text{O}$  and  $\delta^{13}\text{C}$ , respectively.

[6] Total carbon, total organic carbon and total nitrogen were determined by means of a LECO CNS analyzer [*Schäfer*, 2005].

[7] AMS radiocarbon dating was performed on carbonaceous shells of *N. pachyderma sinistralis* at the Leibniz-Laboratory for Radiometric Dating and Isotope Research at the Christian Albrecht University in Kiel, Germany. <sup>14</sup>C ages have been converted to calendar ages using the CalPal online software (<http://www.calpal-online.de>) with the CalPal2005\_SFCP calibration curve and a correction for the reservoir effect of 420 years (Table 1).

## 3. Stratigraphy

[8] A first characterization of the age of the Hinlopen/Yermak Megaslide has been presented by *Winkelmann et al.* [2006a] which was mainly based upon AMS radiocarbon dates directly below and above the slide-related turbidite in core PS66/309-1. The slide's minimum age was defined by the closest AMS date above the turbidite. This minimum age around 30 calendar (cal) kyr B.P. still represents the best datum of the slide's actual age. However, for further characterization of the trigger mechanism (e.g., timing and trends in environmental conditions), the stratigraphy of this study has been focused on MIS 3. The final age model of core PS66/309-1 KAL was deduced from its oxygen and carbon isotope records (Figure 2), which, in general, can be correlated with the global isotope curve SPECMAP stack [*Martinson et al.*,

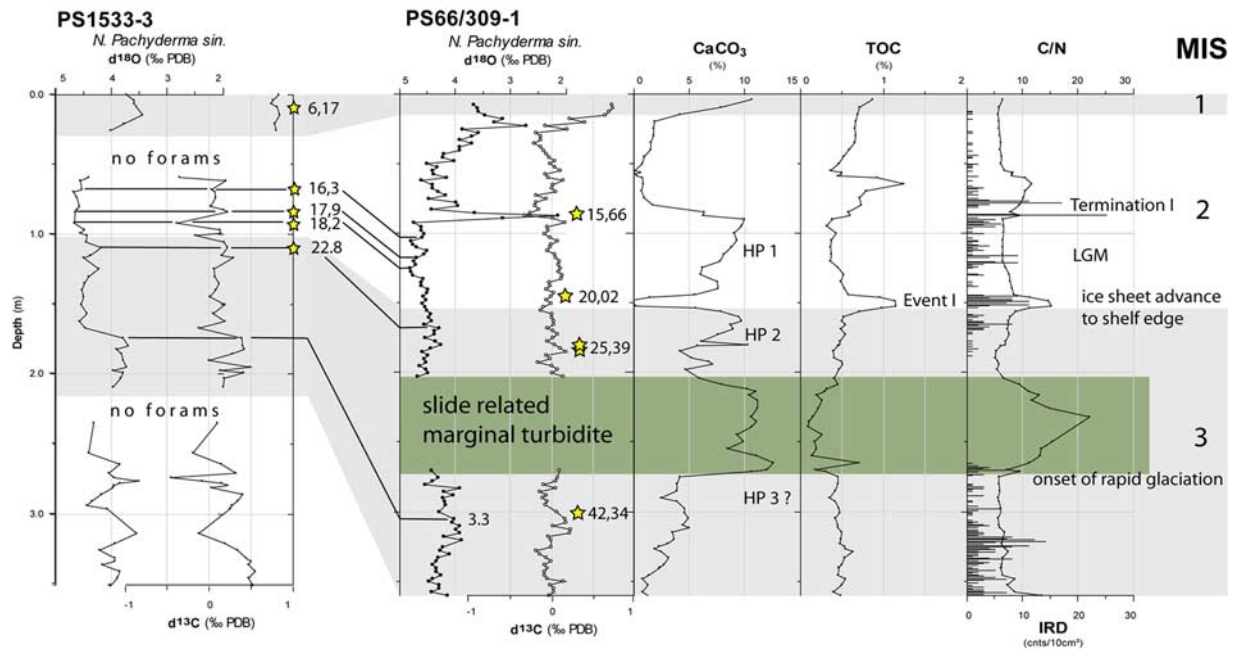


**Figure 2.** Proxy record of core PS66/309-1 KAL including bulk parameter and IRD for MIS 3 within Sophia Basin showing heavy stable oxygen isotope values above 4‰, relatively high carbonate contents during onset of Late Weichselian Glaciation, and Hinlopen/Yermak Megaslide failure event. The advance to the shelf edge by the SBIS is reflected in Event I at the MIS 3/2 boundary. The interval of the Hinlopen/Yermak Megaslide failure event (marginal turbidite, green box [cf. Winkelmann *et al.*, 2006a]) follows a sudden drop to heavy  $\delta^{18}\text{O}$  values around 45 kyr B.P. (MIS substage 3.3). This drop might indicate the onset of the rapid glaciation. HP events (1–3) according to Hald *et al.* [2001]. The chronostratigraphy of core PS66/309-1 KAL is based on the  $\delta^{18}\text{O}$  and  $\delta^{13}\text{C}$  record of *N. pachyderma sin.*, the correlation to core PS1533-3 [Spielhagen *et al.*, 2004], and AMS radiocarbon dating. Marine Isotope Stage (MIS) assignments are based on Martinson *et al.* [1987]. AMS- $^{14}\text{C}$  dates from PS1533-3 [Nørgaard-Pedersen *et al.*, 2003; Spielhagen *et al.*, 2004] are correlated to PS66/309-1 KAL (left; corrected  $^{14}\text{C}$ -kyr). New AMS- $^{14}\text{C}$  dates (right; given in uncorrected  $^{14}\text{C}$ -years B. P.) were measured on *N. pachyderma sin.* at the Leibniz Laboratory, Kiel University.

1987]. AMS  $^{14}\text{C}$  dates at 90, 143, 180, 183 and 300 cm core depth helped to pinpoint Marine Isotope Stages (MIS) 2 and 3. The stratigraphic framework is further supported by correlation to core PS1533-3 and PS2212-3 KAL which have established age models ranging from MIS 1 into 6 [Spielhagen *et al.*, 2004; Vogt *et al.*, 2001] (Figure 2). In core PS66/309-1 KAL a series of meltwater peaks characterize the MIS 2. We date the most prominent peak at  $15,660 \pm 70$   $^{14}\text{C}$ -kyr B.P. ( $18,541 \pm 237$  cal kyr B.P.; Figure 2). Well-dated meltwater events during Termination I have been recognized in the adjacent areas [cf. Hebbeln *et al.*, 1994]. The MIS 3/2 boundary is characterized by a well defined association of sedimentological, mineralogical and organic-geochemical parameters in all sediment cores in the region [cf. Andersen *et al.*, 1996; Vogt *et al.*, 2001] (Figure 2). The layer exhibits lamination and contains high amounts of mature terrestrial organic material and

very low carbonate contents [Vogt *et al.*, 2001]. This layer has been described as Event I [Knies and Stein, 1998] and has been deposited between 22.5 and 19.5  $^{14}\text{C}$  kyr B.P. as based on several AMS  $^{14}\text{C}$ -ages. In core PS66/309-1 KAL the closest AMS  $^{14}\text{C}$  date directly above this layer gives an age of  $20,020 \pm 140$   $^{14}\text{C}$  kyr B.P. ( $21,527 \pm 486$  cal kyr B.P., Table 1, Figure 2). According to the published interpretation, we assume it to be a synchronous deposit and use it as one indicator of the lowermost MIS 2 (Figure 2).

## 4. Paleoenvironmental Setting for the Triggering of the Hinlopen/Yermak Megaslide

### 4.1. Late Weichselian Glaciation

[9] A drop to heavy  $\delta^{18}\text{O}$  preceding the megaslide (Figure 2) indicate the preslide onset of glaciation

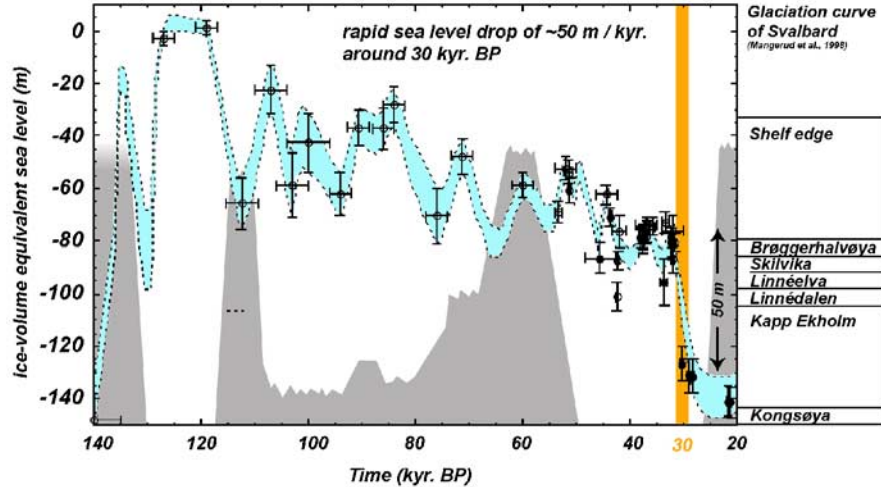


**Figure 3.** Sea level curve (light blue) showing a drastic drop in global sea level around 30 kyr B. P. during the time window of the Hinlopen/Yermak Megaslide (modified from *Lambeck et al.* [2002] with permission from Elsevier) and Glaciation curve of Svalbard (according to *Mangerud et al.* [1998], modified with permission from Elsevier).

and increasing ice volume with its implication for sea level changes. Global sea level data suggest a rapid approach of near maximum volumes around 30 cal kyr B.P. [e.g., *Lambeck et al.*, 2002]. The rapid establishment of maximum ice volume and extent of this Late Weichselian Glaciation, which has been the largest of the Weichselian ones on Svalbard, is documented as strong IRD peaks accompanied by higher sedimentation rates, C/N ratios and TOC contents. This integrated signal occurs around 23.4 cal kyr B.P. when the outlet glaciers reached the shelf edge and postslide intensive terrigenous sediment input commenced (Event I according to *Knies and Stein* [1998]; Figure 2). The Hinlopen/Yermak Megaslide occurred around 30 kyr B.P. Thus it coincides with the transition from the Kapp Ekholm Interstadial into glaciation G of the Svalbard glaciation curve, i.e., the onset of the major Late Weichselian glaciation that lead to maximum extents of the Last Glacial Maximum (LGM) (Figure 3) [*Mangerud et al.*, 1998; *Svendsen et al.*, 2004].

[10] The major element driving this rapid glaciation has been attributed to the higher influx of Atlantic water masses leading to open water conditions and the corresponding moisture supply to buildup of the SBIS [e.g., *Hebbeln et al.*, 1994; *Dokken and Hald*, 1996]. Paleoceanographic proxies show a high productivity zone (HP 2) and point to an increased warm water influx to the area west and north of Spitsbergen between 32 and 26 cal kyr B.P. [*Dokken and Hald*, 1996; *Hald et al.*, 2001; *Hebbeln et al.*, 1994, 1998; *Spielhagen et al.*,

2004]. The associated meridional surface circulation pattern (paleo-WSC) might have not differed drastically from the modern pattern [e.g., *Hebbeln et al.*, 1998].

#### 4.2. Eustatic Versus Isostatic Sea Level Changes on Svalbard

[11] The paleo-sea level and isostatic position of Svalbard is a crucial factor in discussing the possible trigger mechanisms of the megaslide. Sea level changes (Figure 3) directly influence the pressure field, buoyancy and thus stability of sediments as well as hydrate stability. The assessment of an isostatic sea level and position of the paleoshoreline of North Spitsbergen is, however, complicated. Raised beaches (for location of sites see Figure 4) have been found, e.g., on Reinsdyrflya at 90 m a.s.l. [*Salvigsen and Österholm*, 1982] and on the west coast of Phippsøya at 20 m a.s.l. [*Forman and Ingólfsson*, 2000] with ages >40 <sup>14</sup>C kyr B.P., at the south shore of Isfjorden dated to 36 <sup>14</sup>C kyr B.P. [*Mangerud et al.*, 1992], on northern Prins Karls Forland at 30 to 40 m a.s.l. with ages between 30 and 40 <sup>14</sup>C kyr B.P. [*Andersson et al.*, 1999]. A morainic ridge in Lifdefjorden contains sublittoral sands below the till and date to 36 <sup>14</sup>C kyr B.P. [*Landvik et al.*, 1998]. Raised marine sediments below a till bed in Linnédalen, west Spitsbergen gave ages of 40 and 36 <sup>14</sup>C kyr B.P. The youngest radiocarbon dates below the LGM associated till on northwest Spitsbergen of calcereous algae gives 33.9 <sup>14</sup>C kyr B.P. while the

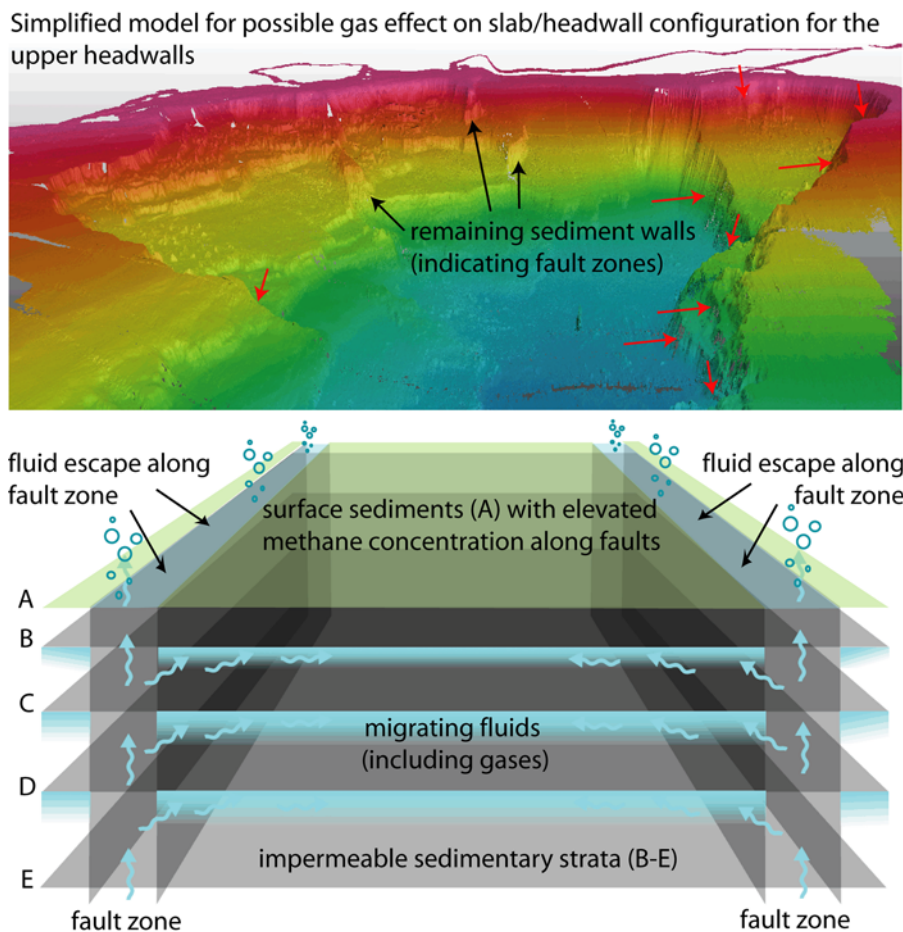


**Figure 4.** Simplified effect of fluids and gases migrating along structures (fractures and faults, especially major fault zones) within the sedimentary strata on the geometry of sediment slabs that are prone to failure. The model included two processes, both identified on the continental shelf of western Svalbard: (1) fluid escape and venting of gases along structures on the seafloor as reported by *Knies et al.* [2004] and (2) accumulation of gases or gas hydrates along sedimentary strata bound by major fault zones as described by *Vanneste et al.* [2005]. The remaining seafloor topography after a slide-related evacuation will include exposed glide planes (representing the sediments directly below the weakened layers) and outstanding sediment walls (that represent sediment bound by fault zones that were able to release the fluids and gases). Both morphological features can be seen in the 3-D model in the background showing the multiple headwalls of the Hinlopen/Yermak Megaslide (view from the north; high-resolution bathymetry data of *Vanneste et al.* [2006]). Black arrows indicate remnant sediment walls. Red arrows indicate distinct planar elements (faults) that define the geometry of headwalls and sidewalls. Note the sharp and steep flanks on the lower right. These sidewalls constitute prolongations of the Hinlopen Fault Zone (striking almost NNW-SSE).

youngest marine fossils incorporated in the till date to 28.5 <sup>14</sup>C kyr B.P. [*Landvik et al.*, 1998].

[12] Summarizing the terrestrial geologic evidence, Svalbard must have experienced an isostatic sea level rise prior to 30 cal kyr B.P. (Kapp Ekholm Interstadial [cf. *Mangerud et al.*, 1998]) and a following drastic drop before the LGM. In Linnédalen a local sea level drop of at least 87 m can be inferred from raised marine sediments in a terrace at 87 m a.s.l. [*Mangerud et al.*, 1998]. However, precise information on both local isostatic sea level

and shorelines on north Spitsbergen are not available so far. Thus the discussion on changes in the pressure field (from relative sea level changes) and consequently increasing or decreasing buoyancy of the sediment prone to failure is dependent on information of the global sea level.

[13] *Lambeck et al.* [2002] defined the onset of the LGM as the time when sea level first approached their minimum levels at ~30 cal kyr B.P. The LGM ice volumes were approached at about 30 cal kyr B.P. too and increased only slowly during the



following 10 kyr (Figure 3). The onset of the LGM was thus accompanied by a rapid fall in sea level with  $\sim 50$  m in less than 1000 years. A similar high rate in falling sea level has only been reported for an interval during the early MIS 3 (Figure 3). The subsequent cold period leading into the LGM was characterized by rapid oscillations in sea level, with magnitudes of tens of meters in time intervals of 1000 years or less. These oscillations were superimposed on a gradually falling sea level [Lambeck *et al.*, 2002].

[14] The direct consequence of such a sea level drop is a change in the pressure field within the TMF sediments by approximately  $-500$  kPa ( $502.7$  kPa; equivalent to 50 m of sea level drop) resulting in a decrease in buoyancy by 0.21% of a single particle with given volume at 2000 m modern water depth (MWD).

[15] This possible change in buoyancy of  $-0.21\%$  results in a higher gravity-driven particle support within the sediments leading to increased stability in an open (connected pores) particle-supported system (e.g., sand). Under sealed conditions, or semi-sealed conditions within clay-rich sediments (pore volume is less efficiently connected), a drop in water column pressure (sea level drop) can result in hydrostatic overpressure within the pore space, thus reducing the shear strength of the sediment. The pressure equilibration within the pore volume is dependent on the permeability of the actual sediments and might be retarded accordingly, especially between sedimentary strata of different physical properties (e.g., clay rich sediments with varying grain size spectra). Therefore elevated pore water pressure might have contributed to reduced stability, even though this contribution appears comparably small at 2000 m water depth. Considering the nature of the TMF sediments (glacigenic debris flows), most of them deposited during active glacial discharge from the Hinlopen ice stream [Ottesen *et al.*, 2005] a drop in pressure should approach conditions under which these sediments have been deposited (lowered sea level during major glaciations), thus stabilizing them.

[16] However, these considerations are based on the calculated compressibility of seawater which is very small and usually neglected for a porous media (even if it is characterized by a very low permeability) and long-term processes like sea level changes. A falling sea level should therefore be directly accompanied by a decrease of the total stress and the hydrostatic pressure proportional to the sea level drop. Thus the sea level drop should

not have generated excess pore pressure in the submerged and saturated TMF sediments, and therefore it cannot be considered as the slope triggering mechanism. However, in the case of dissolved or free gas or hydrate phases within the pore volume, the pore pressure would be very sensitive to pressure changes, generating excess pore pressure for a falling sea level scenario.

### 4.3. Stability of Potential Gas Hydrates

[17] Given the presence of gas hydrates on Svalbard [e.g., Vanneste *et al.*, 2005] and the potential presence within the TMF sediments before failure, both falling sea level and higher water temperatures could have contributed to a lowering of the hydrate stability zone (HSZ) and may have affected the slope stability of the headwall region north of Spitsbergen.

[18] The relationship of methane and/or gas hydrates to submarine slides is in contrast to other possible causes so far hypothetical. One of the best studied submarine slides that was extensively investigated toward this relationship is the Storegga Slide off Mid Norway [e.g., Mienert *et al.*, 2005a, 2005b; Sultan *et al.*, 2004]. Despite these investigations, a clear causal relationship could not be established so far. Mienert *et al.* [2005b] tried to relate ocean warming of the upper layer to destabilization of hydrates within the headwall area of the Storegga Slide. The calculated change within the pressure and temperature field due to ocean warming for the Storegga Slide [Mienert *et al.*, 2005b] probably lead to an displacement of the HSZ between 400 to 750 m of modern water depth (MWD). This change was accomplished between 12 and 9 cal kyr B.P., well before the Storegga Slide (8.2 cal kyr B.P.). However, Mienert *et al.* [2005b] demonstrated that gas hydrate melting on top of the hydrate occurrence zone (HOZ) could have an essential impact on slope stability in relation to giant submarine slides.

[19] Considering a similar scenario for the Hinlopen/Yermak Megaslide, we can take the modern circulation pattern as an analogue for the warm water inflow north of Svalbard around 30 cal kyr B.P. (end-member scenario). The warm waters would have flushed the outer shelf and thus affected sediments in depth down to 400 m. This excludes the thermally forced hydrate destabilization as the trigger since the initial slope failure of the retrogressive Hinlopen/Yermak Megaslide was positioned well below ( $>2000$  m MWD) this impacted shelf area.



[20] However, the warm waters might have had an impact on (potential) gas hydrates within the upper headwall areas. The warming of these sediments could have led to reduced thickness of the HSZ thus leading to a shoaling of the bottom of the (hypothesized) HOZ with associated possible hydrate melting on its top. In analogue to the Storegga Slide, this scenario would have contributed to instability within the upper headwall area (400–200 m) impacting horizons that were to fail. Especially the geometry of detached sediment slabs during failure might have been affected by this process.

[21] A model that incorporates the knowledge on gas hydrate evidence around Svalbard is given in Figure 4. The gas would migrate along structures like fractures and fault zones [e.g., Knies *et al.*, 2004] to finally escape to the surface, where it is recordable within clayey surface sediments due to adsorption effects. The sediments between these structures act as barriers and according to their physical properties, they allow gas to migrate into distinct horizons as has been reported by Vanneste *et al.* [2005]. The consequence during a major slope failure like the Hinlopen/Yermak Megaslide would be that slabs with their geometries defined by structures and weak horizons (possibly weakened by over-pore pressure from hydrate melting and/or gas enrichment) would slide out in a retrogressive style following an initial failure. The headwall area especially in the eastern part provides morphological evidence of such a scenario (Figure 4).

[22] However, in deeper water depths (no direct impact of warm surface waters; in our case >400 m MWD) the HSZ is pressure-controlled [e.g., Mienert *et al.*, 2005b]. In contrast to the Storegga Slide environmental condition with accomplished ocean warming (12–9 cal kyr B.P.) during a sea level rise (most of it preceding the failure), the Hinlopen/Yermak Megaslide occurred during rapidly falling sea level (50 m/ < 1 kyr [Lambeck *et al.*, 2002]) and ocean warming. Therefore the effects of lowered pressure and ocean warming both result in a thinning of the HSZ with consequent destabilization of possible gas hydrates. The drastic sea level drop of at least 50 m in less than 1 kyr [Lambeck *et al.*, 2002] could have had an influence on the HSZ in the lower part of the preslide slope too, thus being interesting for the trigger mechanism.

[23] Missing the relevant information on sediment properties, geothermal gradient, pressure distribution and gas composition, the calculation of a

hypothetical gas hydrate stability field (GHSF) remains speculative. However, assuming lithostatic pressure distribution for the preexisting Hinlopen TMF and taking  $-0.8^{\circ}\text{C}$  of modern bottom water temperature [Schauer *et al.*, 2004] as well as the Storegga Slide area as an analogue (assuming methane hydrate, a geothermal gradient of  $0.056^{\circ}\text{C}/\text{m}$  for lithostatic pore pressure and application of associated parameters [cf. Bouriak *et al.*, 2000, 2003]), we can calculate a possible GHSF depth as a function of pressure and temperature (Figure 5a).

[24] The relatively fast sea level drop of 50 m would have caused the base of the GHSF to ascend. The lower boundary of the GHSF would have shallowed by  $\sim 21$  m (163 to 142 m subbottom depth), 7 m (250 to 243 m subbottom depth) 5 m (296 to 291 m subbottom depth) and 2 m (351 to 349 m subbottom depth) at 400, 800, 1200 and 2000 m MWD, respectively (Figure 5a).

[25] The resulting higher pore pressure from dissociating gases might certainly have contributed to a possible destabilization of sedimentary strata. Considering the amount and geometry of destabilized gas hydrates, a causal relation to the megaslide appears reasonable. Contrary, the geometry of evacuated slabs (upper headwall heights up to 600 m) does not coincide with the calculated lower boundary of the GHSF (163 to 256 m subbottom depth between 400 and 800 m MWD; Figure 5b) and might confirm that neither an ascending GHSF base nor its an descending top (from surficial thermally induced melting) did configure the detached slabs. The initial slope failure, however, must have been positioned even deeper (between 2000 and 2300 m MWD (D. Winkelmann *et al.*, Dynamic and timing of the Hinlopen/Yermak Megaslide north of Spitsbergen, Arctic Ocean, submitted to *Marine Geology*, 2007; hereinafter referred to as Winkelmann *et al.*, submitted manuscript, 2007)) and below the calculated GHSF base.

[26] However, these considerations should be regarded with care since no information on the real thermal gradient, the (paleo-TMF) sediment's properties, gas composition and pressure distribution are available. Especially the thermal gradient and the sedimentary properties might vary significantly. Furthermore, the applied formula for the methane-seawater-hydrate equilibrium curve [Bouriak *et al.*, 2000] is only valid within the temperature range of  $-2^{\circ}\text{C}$  to  $15^{\circ}\text{C}$ . In addition, this hydrate hypothesis remains theoretical since in contrast to the Storegga Slide area neither bottom

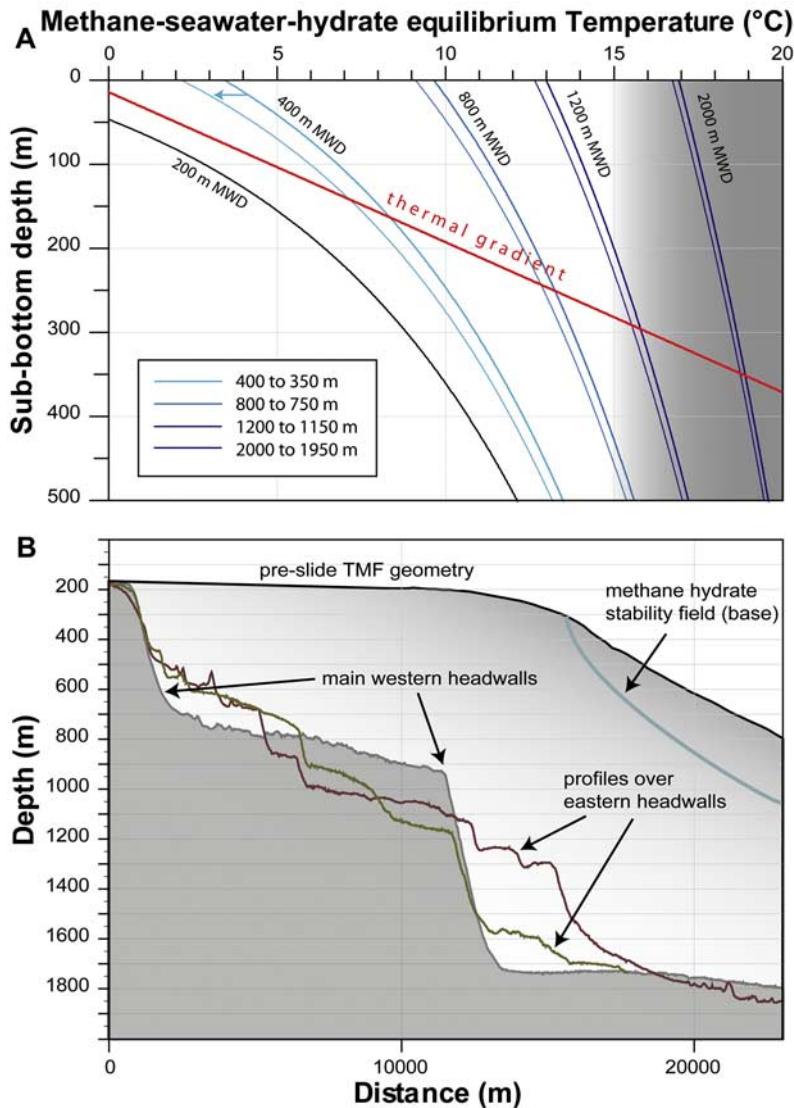


**Figure 5.** (a) Methane-seawater-hydrate equilibrium temperature (MSHT) curves at 400, 800, 1200, and 2000 m modern water depth (MWD) before and after a 50 m sea level drop. For MSHTs below the thermal gradient, instability for methane hydrates can be expected. (b) Bathymetry profiles across the main western (gray) and eastern (brown and olive) headwalls in relation to preslide bathymetry of the TMF with indicated methane hydrate stability zone. Note that the headwall geometries and depths do not coincide with the gas hydrate stability field (GHSF).

simulating reflectors (BSRs), degassing features nor other evidence of free gas or gas hydrates have been recognized so far north of Spitsbergen that would corroborate it.

[27] Additional doubt on the gas hydrate hypothesis as the slide trigger comes from another consideration. Large amounts of gas (in case of the potential hydrate north of Svalbard mainly methane) hydrates would have been necessary to destabilize the Hinlopen TMF in a sufficient way to reach such a shelf collapse. If large amounts of methane clathrates would be involved in a subma-

rine slide [cf. Paull *et al.*, 2003], an altered isotopic signature ( $\delta^{13}\text{C}$  of methane is  $< -60\text{‰}$  versus PDB) can be expected in the dissolved carbon pool of the (local) ocean recorded as peaks in foraminiferal tests [e.g., Smith *et al.*, 2001; Millo *et al.*, 2005]. The  $\delta^{13}\text{C}$  record of planktic *N. pachyderma sin.* from nearby cores does not show light  $\delta^{13}\text{C}$  events and thus indication of a bigger methane release (Figure 2).

[28] Whether or not gas hydrates contributed to the Hinlopen/Yermak Megaslide, however, remains unclear. Despite the fact that methane was found

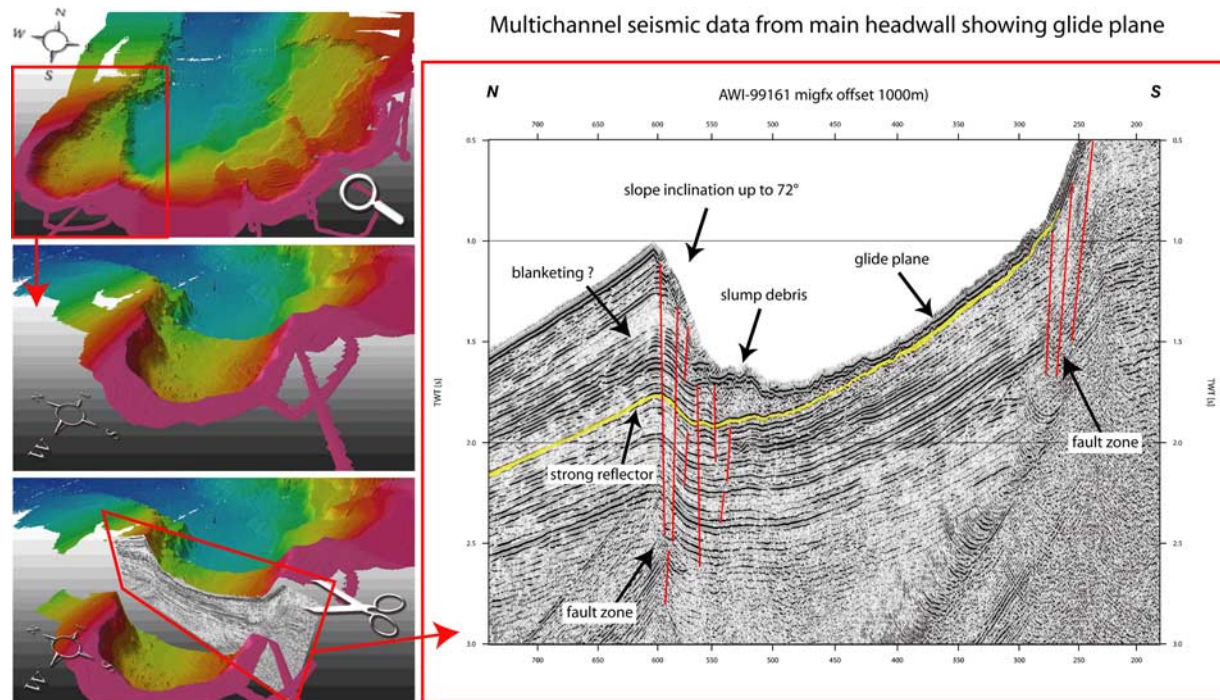


**Figure 6.** Seismic line AWI-99161 across the main headwall of the Hinlopen/Yermak Megaslide showing slide debris on glide plane which can be traced into the adjacent fan sediments of the old Hinlopen Trough Mouth Fan. There it constitutes a strong reflector. Note that the evacuated sediment slab is bound by fault zones. The indicated blanketing results at least partly from AGC filtering. See 3-D model (view toward NE) on the left for location (seismic data from *Geissler and Jokat* [2004]; bathymetry data from *Vanneste et al.* [2006]).

to be concentrated along major geological structures on west Spitsbergen [e.g., *Knies et al.*, 2004], hydrate accumulation zones are bound by major geological structures [*Vanneste et al.*, 2005] and in contrast to *Cherkis et al.* [1999], who showed a possible BSR in the headwall region, there is no direct evidence for methane, hydrates (BSRs) nor degassing features in or close to the headwall area of the Hinlopen/Yermak Megaslide (Figure 6). The headwall morphology exhibits a strong tectonic control as headwalls and sidewalls can be related to fault zones (Figures 4 and 6). However, considering a complete removal of potential hydrates (as the entire HSZ might have slid away), the absence of proof in our data does not prove absence of hydrates in MIS 3.

#### 4.4. Glaciotectonic Activity

[29] The transition from the Kapp Ekholm Interstadial into glaciation G of the Svalbard glaciation curve [*Mangerud et al.*, 1998] must have been rapidly and accompanied by rapid Ice loading onto the Svalbard archipelago. LGM-related moraines on northwestern Spitsbergen have been described

by *Listøl* [1972]. *Salvigsen* [1977] dated bivalves from marine sediments that have been incorporated into the related till. They display middle Weichselian ages, the youngest of 28.5  $^{14}\text{C}$  kyr B.P. which gives indication for marine transgression at around 33.2 cal kyr B.P. and glacial activity shortly after. Thus an increasing glaciotectonic activity probably characterized the time window of the slide event.

[30] Given the spatial offset from the moisture sources close to the shelf edge and the main deposition centers on Svalbard and the Barents Sea (around Kongsøya [e.g., *Ingolfsson et al.*, 1995; *Lambeck*, 1996; *Svendsen et al.*, 2004]), an uneven loading of ice onto the lithospheric crust in the area can be postulated (Figure 7). The corresponding gradients in load would run from depo-centers near Kongsøya on Svalbard to open waters near the western and northwestern regions of Spitsbergen. Thus areas to the west and to the east of the Hinlopen cross shelf trough might have experienced a different loading history which can be termed asymmetrical. Increasing asymmetrical ice loading during intensification of Late Weichselian Glaciation adjacent to the Hinlopen cross shelf

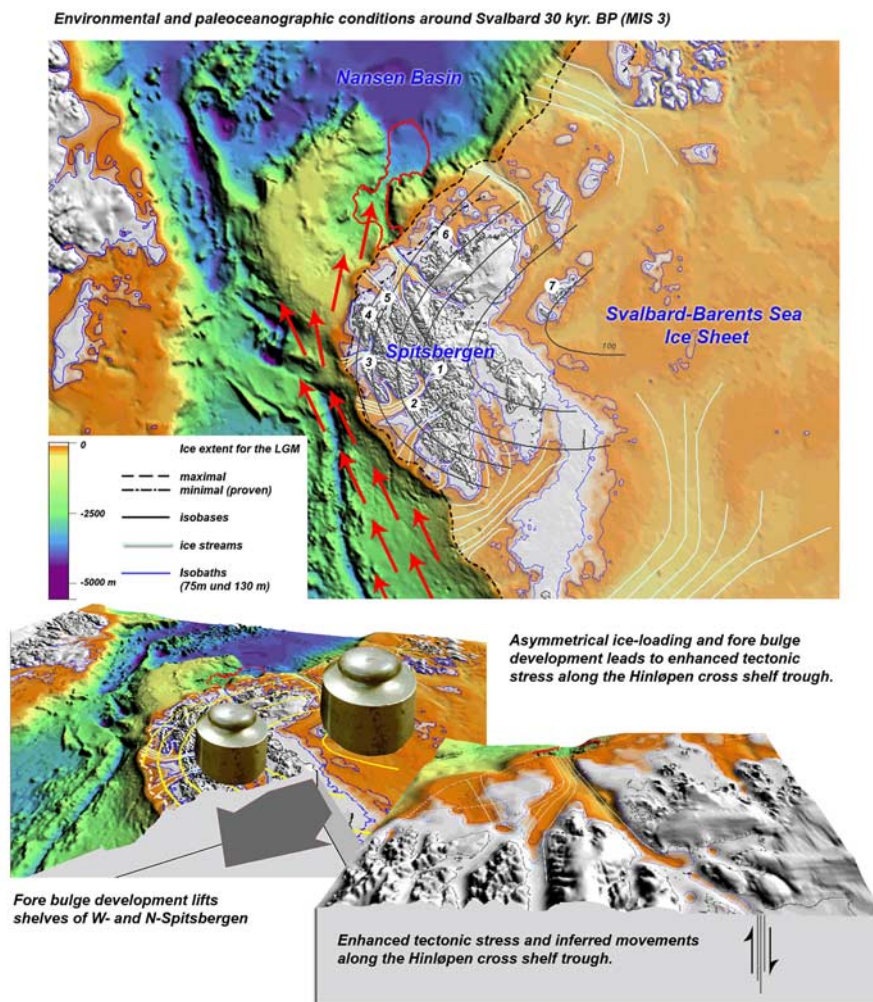


**Figure 7.** Map with paleoenvironment during MIS 3, sea level between  $-75$  and  $-130$  m (according to *Lambeck et al.* [2002]; blue isobaths of today's topography/bathymetry), ice sheet extent close to maximum (LGM, according to *Landvik et al.* [1998]) and isobases fairly indicating LGM depo-centers (based on relative sea level data from post-LGM emergence [*Landvik et al.*, 1998]) ice sheet thickness, oceanic circulation (inflow of Atlantic water masses during HP events, red arrows), and ice streams [*Ottesen et al.*, 2005]. Triggering model for the Hinlopen/Yermak Megaslide showing warm water inflow, increasing asymmetrical ice loading (weights), forebulge development, and inferred movements along the Hinlopen Strait/Hinlopen Trough. (Site names: 1, Kapp Ekholm; 2, Linnédalen/Linnéelva; 3, N Prins Karls Forland; 4, Lifdefjorden; 5, Reinsdyrflya; 6, Phippsøya; 7, Kongsøya.)

trough might have caused an additional tectonic stress along this major fault zone leading to higher mechanical activity in the headwall area. Neotectonic activity and faulting due to subsequent isostatic adjustment following the last deglaciation have been described for Scandinavia and the Baltic Sea [e.g., *Kotilainen and Hutri*, 2004; *Bungum et al.*, 2005].

#### 4.5. Forebulge Development

[31] In addition, the rapid growth of the SBIS must have had an impact on the isostatic equilibrium in

the area. A developing forebulge (Figure 7) is a physical consequence of ice loading onto the lithosphere and probably contributed to the slope instability leading to the Hinlopen/Yermak Megaslide.

[32] However, the lack of reliable information on the lithospheric rheology makes the forebulge assessment a complicated affair. The assessment of local isostatic effects of a forebulge development is heavily dependent on the lithospheric flexural rigidity. Unfortunately, this parameter is not well known and uncertainty on it remains.



*Fjeldskaar* [1994] estimated lithospheric flexural rigidity in Scandinavia to be between  $1 \times 10^{24}$  and  $1 \times 10^{25}$  Nm. *Howell et al.* [2000] applied sensitivity tests for their numerical model for the SBIS during the Late Weichselian Glaciation (including the LGM). Depending on the applied rigidities, the associated forebulges vary between narrow isostatic effects close to the ice load (lithospheric flexural rigidity  $1 \times 10^{24}$  Nm) and wide with no overall uplift within the Barents Sea (lithospheric flexural rigidity  $1 \times 10^{26}$  Nm) in their model. *Howell et al.* [2000] concluded with a possible scenario for the central Barents Sea that forebulge development due to early glaciation from the Arctic archipelagos (including Svalbard) and Scandinavia (80 m) in combination with global sea level fall (120 m) would be capable to expose parts of the central Barents Sea subaerially. This would be enough to form glaciation nuclei on the Central Bank and would have aided grounded ice sheets from Scandinavia and the Arctic archipelagos to merge in the central Barents Sea. This modeled scenario stands in accordance with geomorphological evidence and has been accomplished by application of a rigidity of  $1 \times 10^{25}$  Nm.

[33] Beside the fact that a forebulge is a direct physical consequence of a growing ice sheet, there is additional evidence within the geological archive. At Linnédalen, a terrace at 87 m a.s.l. has been described by *Mangerud et al.* [1998]. The minimum ages of marine sediments below the LGM-associated till gave a finite age of 35.9 <sup>14</sup>C-kyr B.P. Thus the sediments were deposited at a global sea level at  $-80$  m [*Lambeck et al.*, 2002] which results consequently in a depression of west Spitsbergen of at least 167 m around 40 kyr B.P. The lithological sequence at Linnéelva (20–30 m a.s.l. [*Mangerud et al.*, 1998]) shows coarsening upward and shore face sediments just below the LGM-till. This indicates a local (isostatic) sea level drop shortly after marine sedimentation and before the LGM (at least until 22 kyr). Considering the global sea level drop of  $\sim 50$  m (from  $-80$  to  $-130$  m around 30 kyr B.P.), west Spitsbergen should have experienced an uplift of at least 7–17 m to reach sea level at Linnédalen. The actual uplift was probably higher due to the fact that the marine sediments of the 87 m terrace had been deposited well below sea level. This uplift can be interpreted as an indication of a forebulge development around 30 kyr B.P. This interpretation coincides with the latest view on the LGM ice sheet conditions on Spitsbergen, suggesting highly dynamic and focused ice drainage via ice streams and

the existence of nunataks in W and NW Spitsbergen [*Landvik et al.*, 2005]. Sea level records of Svalbard's postglacial emergence (dating of raised beach deposits) indicate a short-lived temporary uplift and following subsidence of sites that were positioned close to the maximum ice sheet extent [*Forman and Ingólfsson*, 2000; *Lambeck*, 1996; *Landvik et al.*, 1998]. This can be interpreted as an indication of a retrograding forebulge.

[34] Considering the possible asymmetrical loading, associated forebulge development might have been different to the west and east of the Hinlopen cross-shelf trough leading to enhanced stress and movements along the fault zone.

#### 4.6. Seismic Rate and Earthquake Amplification

[35] The combination of rapid glaciation and rapid loading on the corner of continental lithosphere has likely played a significant role for the seismic rate too. *Sauber and Molnia* [2004] reported that earthquake frequency and magnitude might be influenced by climatic factors. They showed on data from southern Alaska that melting of glaciers due to global warming is accompanied by reduced loading of the lithosphere, leading to an increase in the number of earthquakes ( $ML \geq 2.5$ ) and seismic rate associated with ice thinning and a decrease in the number of earthquakes and seismic rate associated with ice thickening [*Sauber and Molnia*, 2004]. Thus cooling of the lithosphere in concert with loading from ice sheets and glaciers can be expected to hamper the crustal movements which leads to accumulation of tectonic strain. This process would lead to earthquakes with higher amplitudes on a lower frequency. An earthquake could have been the final trigger leading to failure of the TMF sediments east of the Hinlopen fault zone and to creation of the steep western headwalls of this megaslide.

#### 4.7. Importance of the Rate of Environmental Changes

[36] The Hinlopen/Yermak Megaslide as a single major failure event and its physical configuration as a partial shelf collapse with combined headwalls heights of 1600 m, is a rather unique slide event. Therefore triggering as well as slope stability conditions might be regarded as unique or at least special too. An increasing asymmetrical ice loading and falling sea level seems not enough to explain an apparently singular event. Intensive glaciations have been recorded before the Weichselian [e.g.,



*Svendsen et al.*, 2004] and a similar failure event has not been reported so far. A possible answer to that might be the rapidity of involved processes. The speed of environmental changes is a crucial factor for stability-related processes. An unprecedented speed would be able to exceed a threshold in the stability system resulting in sediments prone to failure. Rapid sea level drop and rapid glaciation with its consequences (forebulge development) for the tectonic activity characterize the time of the Hinlopen/Yermak Megaslide shelf collapse. Finally, the position of the shelf failure on a major fault zone on a continental corner with two extensional stress fields seems a special factor too. In concert with the lithological properties of the glacial/interglacial sediments this factor might explain the enormous headwall heights.

#### 4.8. Favored Triggering Scenario

[37] Following the considerations on environmental conditions, their effects and possible triggers of the Hinlopen/Yermak Megaslide, we can approach a likely triggering scenario.

[38] The pressure induced changes within particle buoyancy (0.21%) appear insufficient for a submarine megaslide. Hydrate destabilization from ocean warming on the upper slope and shelf could not have affected the area of initial failure. Hydrate destabilization from pressure drop cannot be ruled out but appears insufficient to result in megascale failure. In addition, we found no evidence for hydrates (escape features, hydrates, free gas, BSRs, etc.) near the slide. The headwall configuration clearly displays sharp planar elements that defined the slid sediment slabs. The more or less vertical planar elements can directly be related to minor and major structures (fault zones) on the Svalbard archipelago (Winkelmann et al., submitted manuscript, 2007) (Figures 4 and 6). As discussed above, this morphology points to a tectonic control of the Hinlopen/Yermak Megaslide. The fact that part of the former TMF west of the Hinlopen fault zone is still present and exhibits the most stable side and headwalls (including highest inclinations; Figures 4 and 6) corroborates the tectonic control interpretation (if hydrates or pressure and/or temperature changes would be the cause, the full TMF should have failed).

[39] Thus the most probable trigger is to be seen within the spectrum of glaciotectonic activity arising from asymmetrical ice loading and forebulge development. An amplified earthquake along the Hinlopen fault zone positioned near the bottle neck

of the headwall area is the most likely candidate for the final trigger leading to initial failure.

#### 5. Conclusions: Triggering Scenario for the Hinlopen/Yermak Megaslide

[40] The Hinlopen TMF and parts of the adjacent continental slope collapsed around 30 cal kyr B.P. Preconditioning and trigger mechanism appear to be special to explain the unprecedented geometry and physical configuration of the Hinlopen/Yermak Megaslide.

[41] The lithological (climatically controlled) preconditions are (1) intercalation of interglacial and glacial sediments of the Pleistocene strata on the shelf and (2) transition of glaciogenic debris flows of a TMF into normal glaciomarine sediments.

[42] The environmental (climatically controlled) preconditioning of the Hinlopen/Yermak Megaslide include (1) higher influx of warm Atlantic water by the paleo-WSC (HP 2) accompanied by (2) a rapid drop in sea level as inferred from terrestrial geologic evidence as well as global data forcing the (3) HSZ to thin and large isostatic movements along the Hinlopen cross-shelf trough resulting from ice loading of the rapidly growing SBIS.

[43] The changes in sediment buoyancy of  $\sim 0.21\%$  (2000 m water depth) appear to small for explain the initial failure. Excess pore water pressure due to pressure changes within semi or fully closed pore space sediment systems appears unlikely as the trigger since the TMF sediments have been deposited during sea level low stands and should therefore approach equilibrium.

[44] Despite the absence of hydrate indications, we cannot tell from our data whether or not gas hydrates contributed to less slope stability within the preslide Hinlopen TMF. However, gas hydrates might not explain the initial slope failure although they possibly contributed to less slope stability within the upper slope.

[45] Considering that only part of the Hinlopen TMF collapsed (along a major fault zone), theories based on changes in the temperature and/or pressure field fail to explain the stability within the remaining TMF.

[46] Asymmetrical loading on the continent corner by rapid onset of the Late Weichselian Glaciation around 30 cal kyr B.P. accompanied by a forebulge development and a strong earthquake, probably positioned below or close to the bottle neck of



the headwall region probably resulted in unprecedented movements along the Hinlopen cross shelf trough. The subsequent sediment failure along this major fault zone appears to be the favorite triggering scenario for the Hinlopen/Yermak Megaslide. Thus the trigger is external and not internal (lithological, compensating overburden) as has been proposed for other slides.

## Acknowledgments

[47] This study is part of the ESF EUROMARGINS Project Slope Stabilities on Europe's passive continental margins (SPACOMA) and funded by the German Research Foundation (DFG, STE 412/17). We are thankful to the scientific shipboard party and the captain and crew of R/V *Polarstern* during ARK-XX/3. We thank W. H. Geissler for providing the seismic data from the main headwall and M. Vanneste for the bathymetry data of the headwall area.

## References

- Andersen, E. S., T. M. Dokken, A. Elverhøi, A. Solheim, and I. Fossen (1996), Late Quaternary sedimentation and glacial history of the western Svalbard margin, *Mar. Geol.*, *133*, 123–156.
- Andersson, T., S. L. Forman, O. Ingólfsson, and W. Manley (1999), Late Quaternary environmental history of Prins Karls Forland, western Svalbard, *Boreas*, *28*, 292–307.
- Baptista, M. A., P. M. A. Miranda, J. M. Miranda, and L. Mendes Vistor (1998), Constraints on the source of the 1755 Lisbon tsunami inferred from numerical modeling of historical data, *J. Geodyn.*, *25*(2), 159–174.
- Bondevik, S., J. I. Svendsen, G. Johnsen, J. Mangerud, and P. E. Kaland (1997), The Storegga tsunami along the Norwegian coast, its age and runup, *Boreas*, *26*, 29–53.
- Bondevik, S., F. Løvholt, C. Harbitz, J. Mangerud, A. Dawson, and J. I. Svendsen (2005), The Storegga Slide tsunami—Comparing field observations with numerical simulations, *Mar. Pet. Geol.*, *22*, 195–208.
- Bouriak, S., M. Vanneste, and A. Saoutkine (2000), Inferred gas hydrates and clay diapirs near the Storegga Slide on the southern edge of the Vøring Plateau, offshore Norway, *Mar. Geol.*, *163*, 125–148.
- Bouriak, S., A. Volkonskaia, and V. Galaktionov (2003), 'Split' strata-bounded gas hydrate BSR below deposits of the Storegga Slide and at the southern edge of the Vøring Plateau, *Mar. Geol.*, *195*, 301–318.
- Bungum, H., C. Lindholm, and J.-I. Faleide (2005), Postglacial seismicity offshore mid-Norway with emphasis on spatio-temporal-magnitudinal variations, *Mar. Pet. Geol.*, *22*, 137–148.
- Cherkis, N. Z., M. D. Max, P. R. Vogt, K. Crane, A. Midthassel, and E. Sundvor (1999), Large-scale mass wasting on the north Spitsbergen continental margin, Arctic Ocean, *Geo Mar. Lett.*, *19*, 131–142.
- Dokken, T. M., and M. Hald (1996), Rapid climatic shifts during isotope stages 2–4 in the Polar North Atlantic, *Geology*, *24*(7), 599–602.
- Duplessy, J. C. (1978), Isotope studies, in *Climatic Change*, edited by J. Gribbin, pp. 46–67, Cambridge Univ. Press, Cambridge, U. K.
- Fjeldskaar, W. (1994), Viscosity and thickness of the asthenosphere detected from the Fennoscandian uplift, *Earth Planet. Sci. Lett.*, *126*, 399–410.
- Forman, S., and Ó. Ingólfsson (2000), Late Weichselian glacial history and postglacial emergence of Phippsöya, Sjuöyane, northern Svalbard: A comparison of modelled and empirical estimates of a glacial-rebound hinge line, *Boreas*, *29*, 16–25.
- Garcia, E., J. J. Dañobeitia, J. Verges, and PARSIFAL Team (2003), Mapping active faults offshore Portugal (36°N–38°N): Implications for seismic hazard assessment along the southwest Iberian margin, *Geology*, *31*(1), 83–86.
- Geissler, W. H., and W. Jokat (2004), A geophysical study of the northern Svalbard continental margin, *Geophys. J. Int.*, *158*, 50–66.
- Grobe, H. (1987), A simple method for determination of ice rafted debris in sediment cores, *Polarforschung*, *57*(3), 123–126.
- Haflidason, H., R. Lien, H. P. Sejrup, C. F. Forsberg, and P. Bryn (2005), The dating and morphometry of the Storegga Slide, *Mar. Pet. Geol.*, *22*, 123–136.
- Hald, M., T. Dokken, and G. Mikalsen (2001), Abrupt climatic change during the last interglacial-glacial cycle in the polar North Atlantic, *Mar. Geol.*, *176*, 121–137.
- Hebbeln, D., T. Dokken, E. S. Andersen, M. Hald, and A. Elverhøi (1994), Moisture supply for northern ice-sheet growth during the Last Glacial Maximum, *Nature*, *370*, 357–359.
- Hebbeln, D., R. Henrich, and K.-H. Baumann (1998), Paleocceanography of the last interglacial/glacial cycle in the polar North Atlantic, *Quat. Sci. Rev.*, *17*, 125–153.
- Howell, D., M. J. Siegert, and J. A. Dowdeswell (2000), Modelling the influence of glacial isostasy on Late Weichselian ice-sheet growth in the Barents Sea, *J. Quat. Sci.*, *15*(5), 475–486.
- Ingólfsson, O., F. Rögnvaldsson, H. Bergsten, L. Hedenäs, G. Lehmdal, J. L. Lirio, and H. P. Sejrup (1995), Late Quaternary glacial and environmental history of Kongsøya, Svalbard, *Pol. Res.*, *14*, 123–129.
- Jakobsson, M., N. Z. Cherkis, J. Woodward, R. Macnab, and B. Coakley (2000), New grid of Arctic bathymetry aids scientists and mapmakers, *Eos Trans. AGU*, *81*(9), 89, 93, 96.
- Jokat, W. (Ed.) (2000), *The Expedition RKTIS-XV/2 of Polarstern in 1999*, *Ber. Polarforsch. Meeresforsch.*, vol. 368, 128 pp., Alfred-Wegener-Inst., Bremerhaven, Germany.
- Knies, J., and R. Stein (1998), New aspects of organic carbon deposition and its paleoceanographic implications along the northern Barents Sea margin during the last 30000 years, *Paleoceanography*, *13*(4), 384–394.
- Knies, J., E. Damm, J. Gutt, U. Mann, and L. Pinturier (2004), Near-surface hydrocarbon anomalies in shelf sediments off Spitsbergen: Evidences for past seepages, *Geochem. Geophys. Geosyst.*, *5*, Q06003, doi:10.1029/2003GC000687.
- Kotilainen, A., and K.-L. Hutri (2004), Submarine Holocene sedimentary disturbances in the Olkiluoto area of the Gulf of Bothnia, Baltic Sea: A case of postglacial palaeoseismicity, *Quat. Sci. Rev.*, *23*, 1125–1135.
- Lambeck, K. (1996), Limits on the areal extent of the Barents Sea ice sheet in Late Weichselian time, *Global Planet. Change*, *12*, 41–51.
- Lambeck, K., Y. Yokoyama, and T. Purcell (2002), Into and out of the Last Glacial Maximum: Sea-level change during Oxygen Isotope Stages 3 and 2, *Quat. Sci. Rev.*, *21*, 343–360.
- Landvik, J. Y., S. Bondevik, A. Elverhøi, W. Fjeldskaar, J. Mangerud, O. Salvigsen, M. J. Siegert, J. I. Svendsen,



- and T. O. Vorren (1998), The last glacial maximum of Svalbard and the Barents sea area: Ice sheet extent and configuration, *Quat. Sci. Rev.*, *17*, 43–75.
- Landvik, J. Y., Ó. Ingólfsson, J. Mienert, S. J. Lehman, A. Solheim, A. Elverhøi, and D. Ottesen (2005), Rethinking Late Weichselian ice-sheet dynamics in coastal NW Svalbard, *Boreas*, *34*, 7–24.
- Listøl, O. (1972), Submarine moraines off the west coast of Spitsbergen, in *Norsk Polarinstitutt Årbok 1970*, pp. 165–168, Norsk Polarinst., Oslo.
- Mangerud, J., M. Bolstad, A. Elgersma, D. Helliksen, J. Y. Landvik, I. Lønne, A. K. Lycke, O. Salvigsen, T. Sandahl, and J.-I. Svendsen (1992), The last glacial maximum on Spitsbergen, Svalbard, *Quat. Res.*, *38*, 1–31.
- Mangerud, J., T. Dokken, D. Hebbeln, B. Heggen, O. Ingólfsson, J. Y. Landvik, V. Mejdahl, J. I. Svendsen, and T. O. Vorren (1998), Fluctuations of the Svalbard-Barents Sea ice sheet during the last 150 000 years, *Quat. Sci. Rev.*, *17*, 11–42.
- Martinson, D. G., N. G. Pisias, J. D. Hays, J. Imbrie, T. C. Moore, and N. J. Shackleton (1987), Age dating and the orbital theory of the ice ages: Development of a high-resolution 0 to 300,000 years chronostratigraphy, *Quat. Res.*, *27*, 1–27.
- McMurtry, G. M., P. Watts, G. J. Fryer, J. R. Smith, and F. Imamura (2004), Giant landslides, mega-tsunamis, and paleo-sea level in the Hawaiian Islands, *Mar. Geol.*, *203*, 219–233.
- Mienert, J., S. Bünz, S. Guidard, M. Vanneste, and C. Berndt (2005a), Ocean bottom seismometer investigations in the Ormen Lange area offshore mid-Norway provide evidence for shallow gas layers in subsurface sediments, *Mar. Pet. Geol.*, *22*, 287–297.
- Mienert, J., M. Vanneste, S. Bünz, K. Andreassen, H. Haflidason, and H. P. Sejrup (2005b), Ocean warming and gas hydrate stability on the mid-Norwegian margin at the Storegga Slide, *Mar. Pet. Geol.*, *22*, 233–244.
- Millo, C., M. Samthein, H. Erlenkeuser, P. M. Grootes, and N. Andersen (2005), Methane-induced early diagenesis of foraminiferal tests in the southwestern Greenland Sea, *Mar. Micropaleontol.*, *58*(1), 1–12.
- Nørgaard-Pedersen, N., R. F. Spielhagen, H. Erlenkeuser, P. M. Grootes, J. Heinemeier, and J. Knies (2003), Arctic Ocean during the Last Glacial Maximum: Atlantic and polar domains of surface water mass distribution and ice cover, *Paleoceanography*, *18*(3), 1063, doi:10.1029/2002PA000781.
- Ottesen, D., J. A. Dowdeswell, and L. Rise (2005), Submarine landforms and the reconstruction of fast-flowing ice streams within a large Quaternary ice sheet: The 2500-km-long Norwegian-Svalbard margin (57°–80°N), *Geol. Soc. Am. Bull.*, *117*(7/8), 1033–1050, doi:10.1130/B25577.1.
- Paull, C. K., P. G. Brewer, W. Ussler, III, E. T. Peltzer, G. Rehder, and D. Clague (2003), An experiment demonstrating that marine slumping is a mechanism to transfer methane from seafloor gas-hydrate deposits into the upper ocean and atmosphere, *Geo Mar. Lett.*, *22*(4), 198–203.
- Salvigsen, O. (1977), Radiocarbon datings and the extensions of the Weichselian ice-sheet in Svalbard, in *Norsk Polarinstitutt Årbok 1976*, pp. 209–224, Norsk Polarinst., Oslo.
- Salvigsen, O., and H. Österholm (1982), Radiocarbon dated raised beaches and glacial history of the northern coast of Spitsbergen, Svalbard, *Pol. Res.*, *1*, 97–115.
- Sauber, J. M., and B. F. Molnia (2004), Glacier ice mass fluctuations and fault instability in tectonically active Southern Alaska, *Global Planet. Change*, *42*, 279–293.
- Schäfer, C. J. (2005), Untersuchungen zu Menge und Zusammensetzung des Organischen Kohlenstoffs in spätquartären Sedimenten des Yermak-Plateaus (Arktischer Ozean) und Umweltbedingungen, Masters thesis, 105 pp., Univ. of Trier, Trier, Germany.
- Schauer, U., E. Fahrbach, S. Osterhus, and G. Rohardt (2004), Arctic warming through the Fram Strait: Oceanic heat transport from 3 years of measurements, *J. Geophys. Res.*, *109*, C06026, doi:10.1029/2003JC001823.
- Schlichtholz, P., and M. N. Houssais (1999a), An inverse modeling study in Fram Strait, Part 1: Dynamics and circulation, *Deep Sea Res., Part II*, *46*, 1083–1135.
- Schlichtholz, P., and M. N. Houssais (1999b), An inverse modeling study in Fram Strait, Part 2: Water mass distribution and transports, *Deep Sea Res., Part II*, *46*, 1137–1168.
- Smith, L. M., J. P. Sachs, A. E. Jennings, D. M. Anderson, and A. deVernal (2001), Light  $\delta^{13}\text{C}$  events during deglaciation of the East Greenland continental shelf attributed to methane release from gas hydrate, *Geophys. Res. Lett.*, *28*(11), 2217–2220.
- Spielhagen, R. F., K.-H. Baumann, H. Erlenkeuser, N. R. Nowaczyk, N. Nørgaard-Pedersen, C. Vogt, and D. Weiel (2004), Arctic Ocean deep-sea record of northern Eurasian ice sheet history, *Quat. Sci. Rev.*, *23*, 1455–1483.
- Stein, R., (Ed.) (2005), Scientific Cruise Report of the Arctic Expedition ARK-XX/3 of RV “Polarstern” in 2004: Fram Strait, Yermak Plateau and East Greenland Continental Margin, *Rep. Pol. Mar. Res.*, *517*, 188 pp., Alfred Wegener Inst. for Pol. and Mar. Res., Bremerhaven, Germany.
- Sultan, N., P. Cochonat, J.-P. Foucher, and J. Mienert (2004), Effect of gas hydrates melting on seafloor slope instability, *Mar. Geol.*, *213*, 379–401.
- Svendsen, J. I., et al. (2004), Late Quaternary ice sheet history of northern Eurasia, *Quat. Sci. Rev.*, *23*, 1229–1271.
- Vanneste, M., S. Bünz, S. Iversen, and S. Yang (Eds.) (2004), R/V Jan Mayen Cruise Report, NFR Strategisk Universitets Prosjekt (SUP)-Slope Stability, 52 pp., Inst. for Geol., Univ. I Tromsø, Tromsø, Norway.
- Vanneste, M., S. Guidard, and J. Mienert (2005), Bottom-simulating reflections and geothermal gradients across the western Svalbard margin, *Terra Nova*, *17*(6), 510–516, doi:10.1111/j.1365-3121.2005.00643.x.
- Vanneste, M., J. Mienert, and S. Bünz (2006), The Hinlopen Slide: A giant, submarine slope failure on the northern Svalbard Margin, Arctic Ocean, *Earth Planet. Sci. Lett.*, *245*, 373–388.
- Vogt, C., J. Knies, R. F. Spielhagen, and R. Stein (2001), Detailed mineralogical evidence for two nearly identical glacial-deglacial cycles and Atlantic water advection to the Arctic Ocean during the last 90,000 years, *Global Planet. Change*, *31*, 23–44.
- Winkelmann, D., R. Stein, and F. Niessen (2004), The Yermak Slide north of Svalbard (Arctic Ocean)—Preliminary results, paper presented at 2nd EUROMARGINS Conference, Palau de les Heures, Barcelona, Spain, 11–13 Nov.
- Winkelmann, D., W. Jokat, F. Niessen, R. Stein, and A. Winkler (2006a), Age and extent of the Yermak Slide north of Spitsbergen, Arctic Ocean, *Geochem. Geophys. Geosyst.*, *7*, Q06007, doi:10.1029/2005GC001130.
- Winkelmann, D., W. Jokat, F. Niessen, R. Stein, and A. Winkler (2006b), Dynamic and timing of the Yermak/Hinlopen Slide, Arctic Ocean, paper presented at European Geosciences Union General Assembly 2006, Vienna, 2–7 April.